Electronic Supplementary Information (ESI)

for

Structural and dynamical determinants of a β-sheet-enriched intermediate involved in amyloid fibrillar assembly of human prion protein

Luigi Russo,[a] Giulia Salzano,[b,g] Andrea Corvino,[1] Edoardo Bistaffa,[c] Fabio Moda,[c] Luigi Celauro,[b] Gianluca D'Abrosca,[a] Carla Isernia,[a] Danilo Milardi,[d] Gabriele Giachin,[e] Gaetano Malgieri,[a] Giuseppe Legname,[b,f]* and Roberto Fattorusso[a]*

Table of Contents

Figure 1

Figure 2

Figure 3

Figure 4

Figure 5

Figure 6

Figure 7

Figure 8

Figure 9

Figure 10

Figure 11

Figure 12

Figure 13

Figure 14

Figure 15

Figure 16

Table 1

Table 2

Table 3

Table 4

Table 5

Table 6

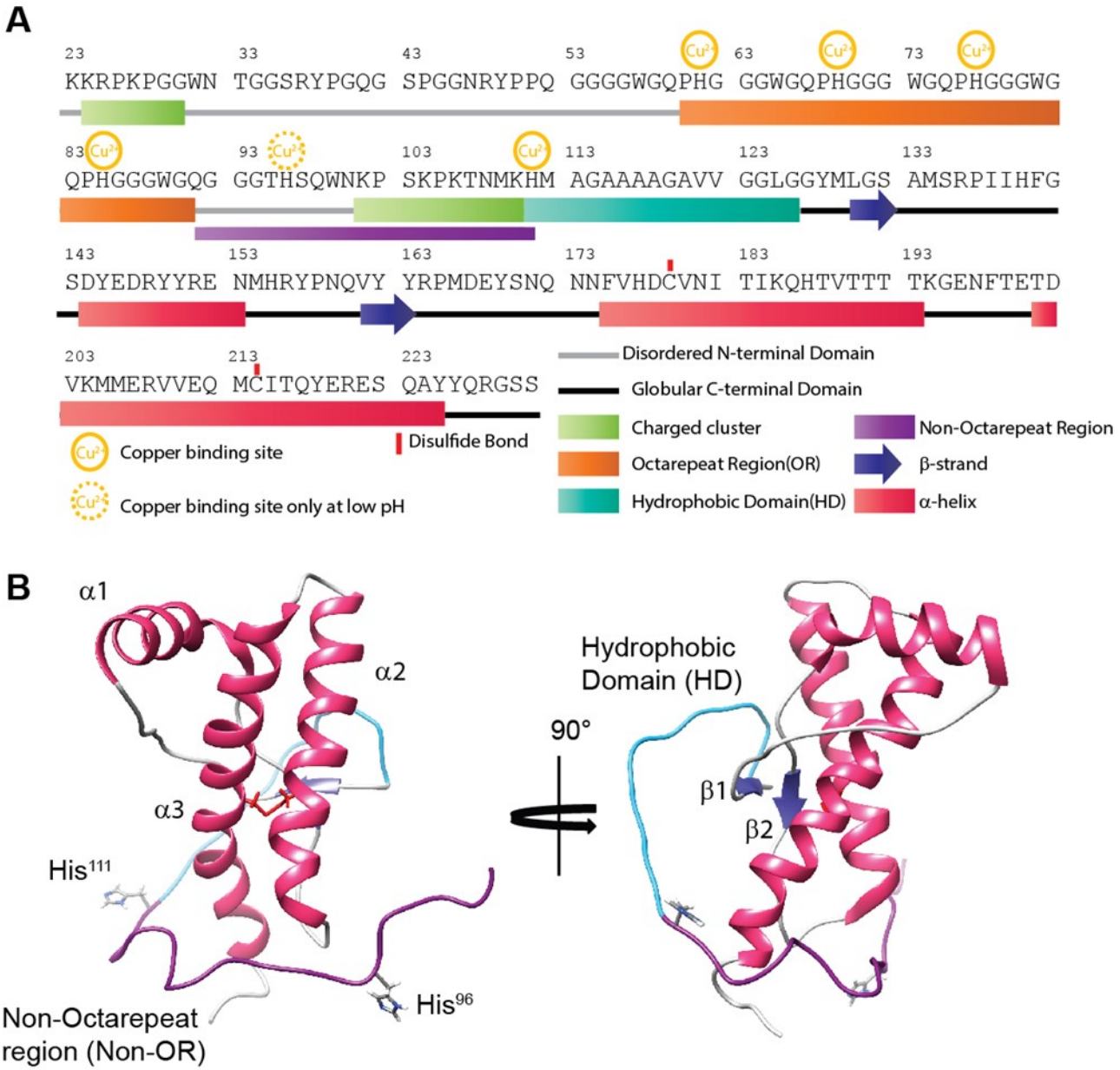

Fig. 1. Structural proprieties of the full-length prion. (A) Schematic representation of HuPrp(23-231) primary and secondary structure. The charged clusters CC1 (residues 24-30) and CC2 (residues 101-110) (light green), the octarepeat region (residues 59-90) (orange), the Hydrophobic Domain (residues 111-126) (cyan), the non-octarepeat region (residues 91-110) (magenta) are also reported. (B) Ribbon drawing representation of the HuPrp(90-231) NMR structure including the C-terminal globular domain. The histidine residues (His^{96}, His^{111}) of the non-octarepeat region are indicated as dark grey stick.

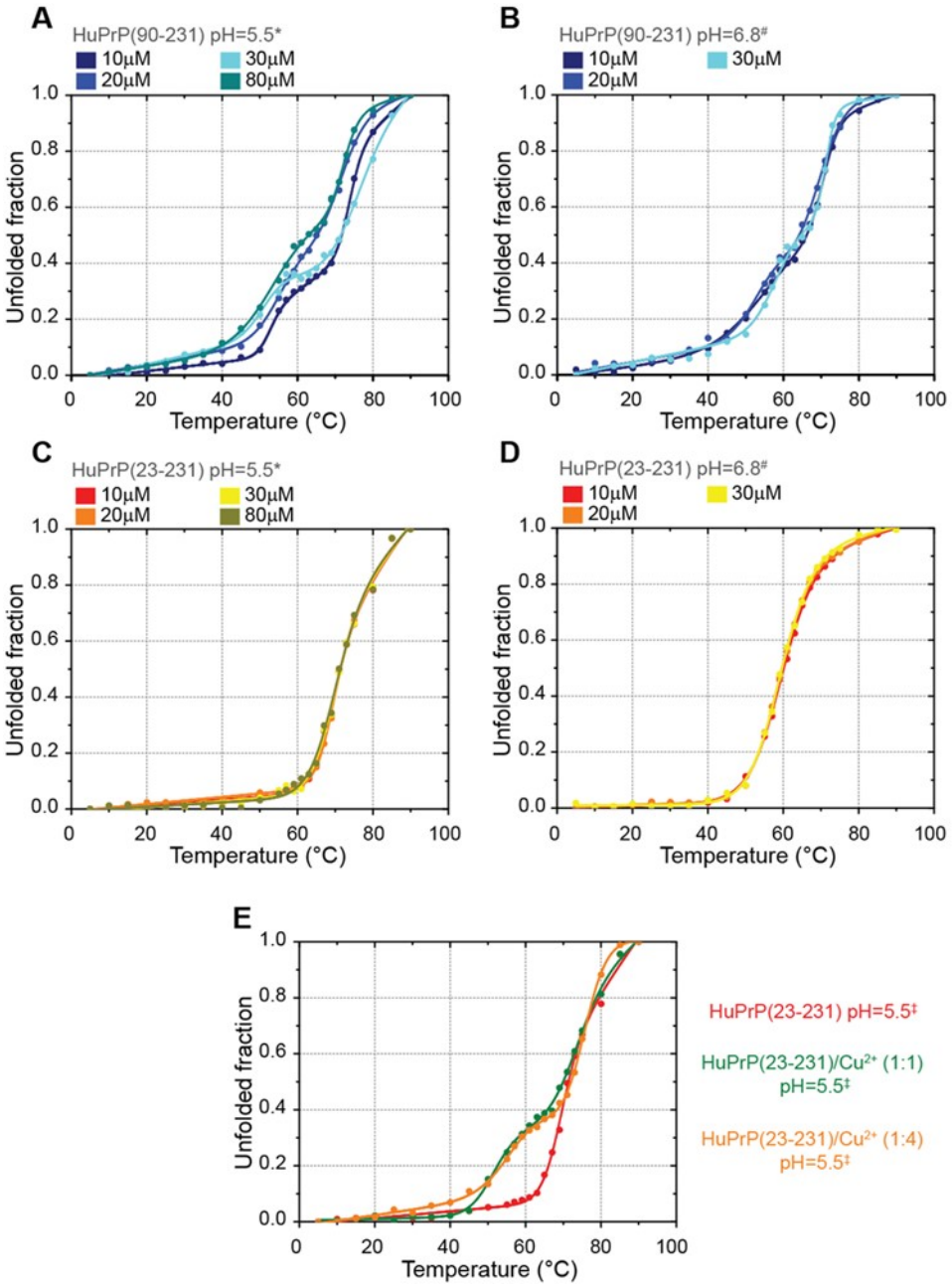

Fig. 2. Thermal unfolding of HuPrP samples followed by CD. Thermal melt plots as function of temperature. Measurements were performed pH 5.5 and 6.8 using acetate* and phosphate# buffer with the same ionic strength. The thermal denaturation of the HuPrP(23-231) in the presence of copper (1 and 4 equivalent(s)) were carried out in MES buffer pH 5.5‡. (A,B) Fraction of unfolded HuPrP(90-231) as a function of temperature and protein concentration at pH 5.5 and 6.8. (C,D) Fraction of unfolded HuPrP(23-231) as a function of temperature and protein concentration at both pH values. (E) Fraction of unfolded HuPrP(23-231) in the absence and in the presence of different copper concentrations (1 and 4 equivalent(s)). The data were fitted by using a two-state model for HuPrP(23-231) in absence of copper and a three-state model for HuPrP(90-231) and HuPrP(23-231)/Cu^{2+}.

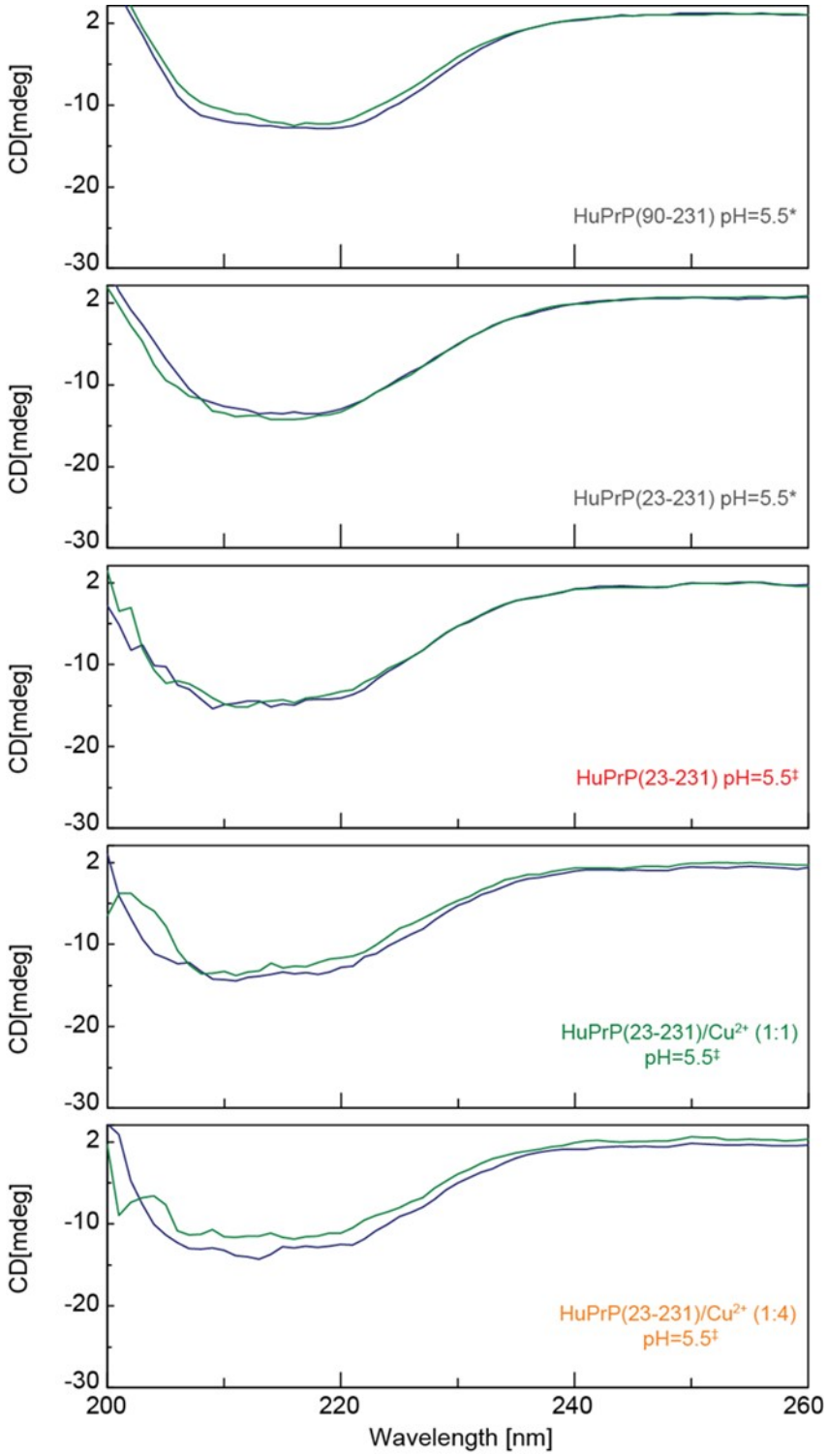

Fig. 3. Unfolding reversibility monitored by CD. Overlaid CD spectra acquired for HuPrP(90-231), HuPrP(23-231), HuPrP(23-231)/Cu^{2+} (1:1) and HuPrP(23-231)/Cu^{2+} (1:4) at pH 5.5 and 10 μM protein concentration. In each case the blue line is for the spectrum recorded at 25 °C; whereas the spectrum obtained after cooling to 25 °C the heat-denatured sample is reported as green line.

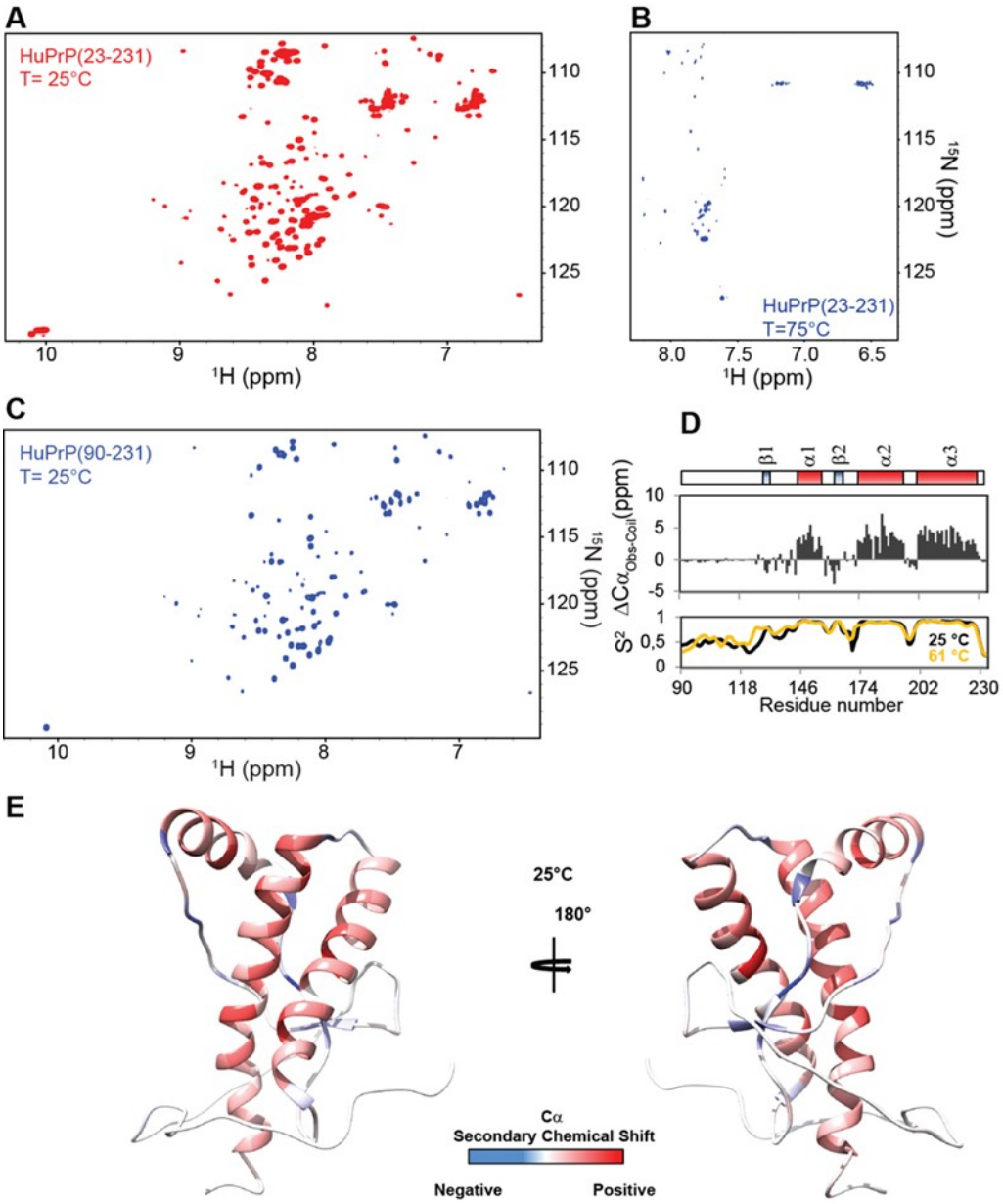

Fig. 4. NMR structural analysis of HuPrP(90-231) and HuPrP(23-231). (A, B) ^{1}H-^{15}N HSQC used to monitor the thermal unfolding of HuPrP(23-231) acquired at 25°C (red) and 75°C (blue) on a 600 MHz spectrometer at pH 5.5. (C) ^{1}H-^{15}N HSQC of HuPrP(90-231) acquired at 25°C pH 5.5 on 600 MHz spectrometer. (D, E) Cα secondary chemical shifts of HuPrP(90-231) at 25°C. The order parameter S^2 obtained by the backbone chemical shift analysis plotted versus the residue numbers at 25°C. Mapping of HuPrP(90-231) Cα secondary chemical shifts onto the NMR structure.

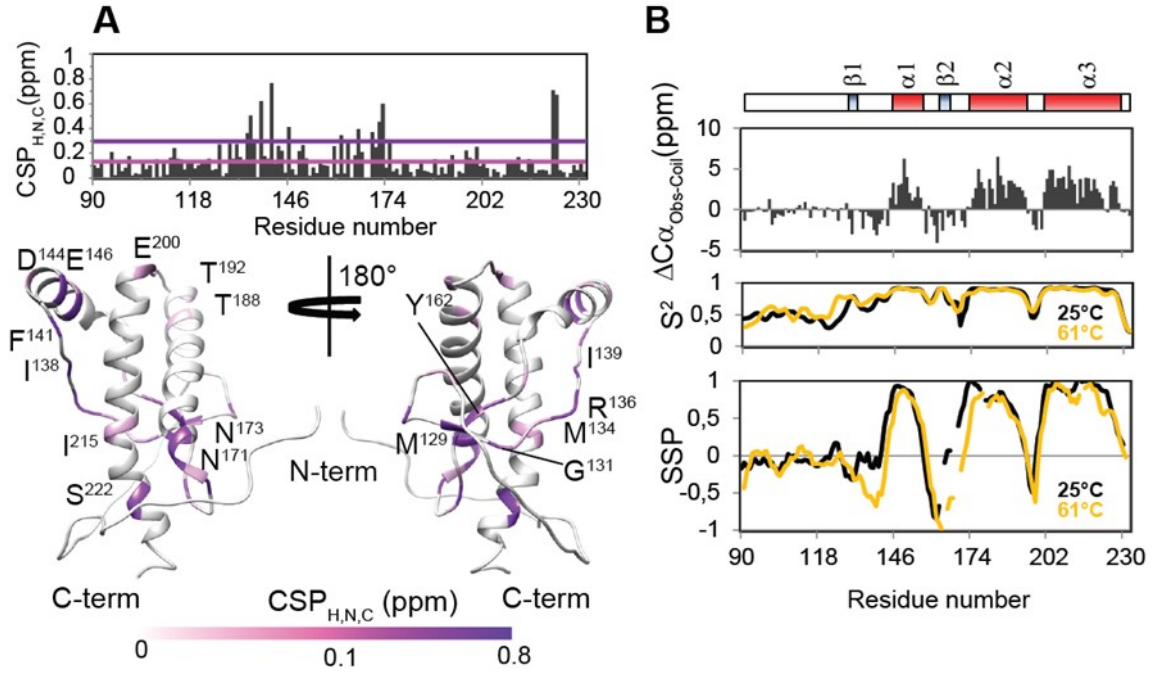

Fig. 5. NMR Structural characterization of the HuPrP(90-231) conformational intermediate state. (A) Structural rearrangements of the C-terminal domain upon temperature increase from 25°C to 61°C as indicated by Chemical Shifts Perturbation (CSP) analysis. CSP values ($\Delta_{H,N,C}$) plotted versus the primary sequence. Mapping of the residues showing significant CSP onto the representative con-former of the HuPrP(90-231) NMR structure (PDB ID: 2LSB). The light pink line indicates the average value (CSP_{avg}) whereas the magenta line reports the CSP_{avg}+ SD value. (B) (upper) Cα secondary chemical shifts of HuPrP(90-231) at 61°C. (middle) S^2 values estimated by using the backbone chemical shifts assigned for HuPrP(90-231) at 61°C. S^2 values are plotted versus the residue number. (lower) The SSP scores (Secondary Structural Propensity) of HuPrP(90-231) at 61°C.

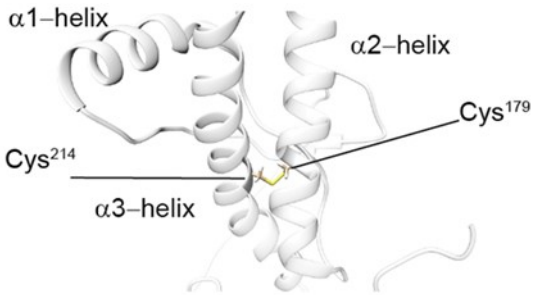

Cα and Cβ chemical shifts (ppm) measured for HuPrP(90-231) at 25° and 61°C

HuPrP(90-231)				
Cysteine	**Cα (25°C)**	**Cα (61°C)**	**Cβ (25°C)**	**Cβ (61°C)**
Cys179	58.8 ± 0.6	57.6 ± 0.6	40.2 ± 0.6	41.1 ± 0.6
Cys214	59.9 ± 0.6	59.8 ± 0.6	41.8 ± 0.6	42.3 ± 0.6
HuPrP(23-231)/Cu^{2+} (1:1)				
Cys179	58.3 ± 0.6	57.4 ± 0.6	41.0 ± 0.6	42.6 ± 0.6
Cys214	60.1 ± 0.6	60.2 ± 0.6	41.8 ± 0.6	42.7 ± 0.6
HuPrP(23-231)/Cu^{2+} (1:4)				
Cys179	58.3 ± 0.6	57.4 ± 0.6	40.8 ± 0.6	42.0 ± 0.6
Cys214	60.2 ± 0.6	61.0 ± 0.6	41.6± 0.6	42.4 ± 0.6

Cα and Cβ reference chemical shifts (ppm) in oxidized and reduced cysteine

Cysteine ^{13}C reference shifts*	**Cα (helix)**	**Cα (beta)**	**Cβ (helix)**	**Cβ (beta)**
Cys(oxidized)	57.6 ± 2.3	54.8 ± 2.1	38.4 ± 3.2	43.0 ± 4.2
Cys(reduced)	62.6 ± 1.7	56.6 ± 1.8	26.5 ± 1.1	29.7 ± 2.0

*The table reports the reference chemical shifts (Mean ± SD) defined by Rajarathnam and co-workers for predicting the redox state of cysteines in a-helix and b-strand.

Fig. 6. Cysteine Cα and Cβ chemical shifts analysis. (upper) close view of the disulphide bridge formed by Cys^{179} and Cys^{214}. The disulphide bond is reported as yellow stick. (lower) The tables report the Cysteine Cα and Cβ chemical shifts measured for the native (25°C) and intermediate states detected at 61°C for HuPrP(90-231) and HuPrP(23-231) in the presence of 1 and 4 equivalent(s) of copper. The cysteine ^{13}C reference values used for predicting the presence of the disulphide bond in the HuPrP(90-231) intermediate state are also reported.

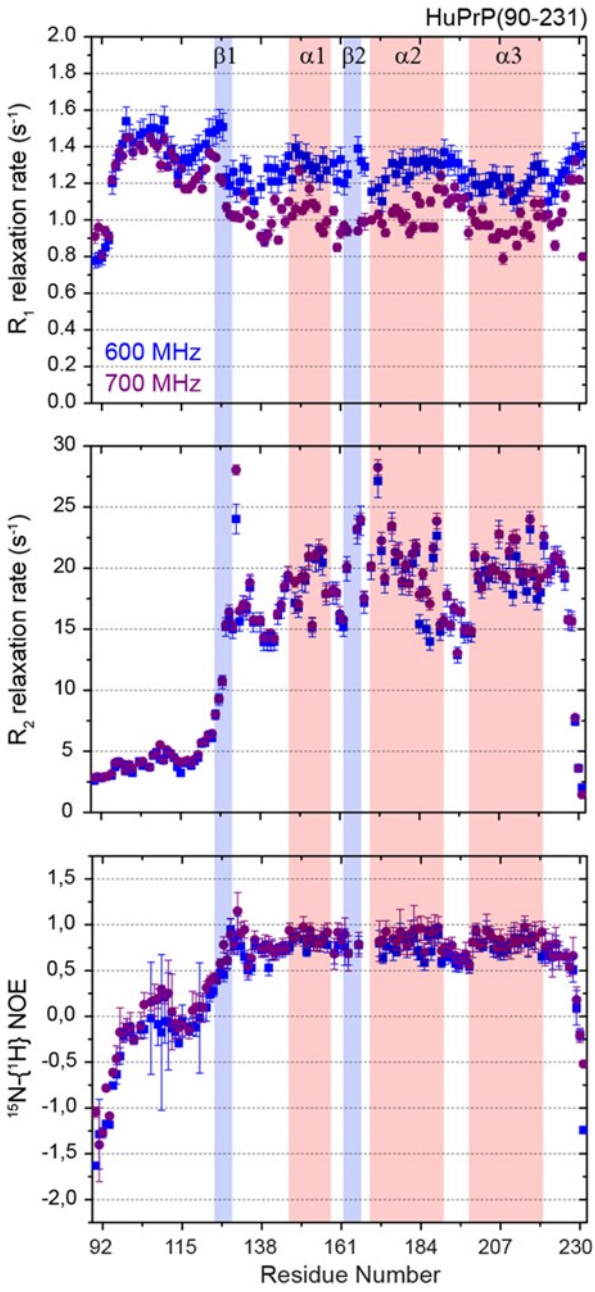

Fig. 7. Backbone dynamics of HuPrP(90-231). ^{15}N longitudinal (R_1) and transverse (R_2) relaxation rates and [^{1}H]-^{15}N heteronuclear NOEs acquired at 298 K. Data were collected at 600 MHz (blue) and 700 MHz (purple).

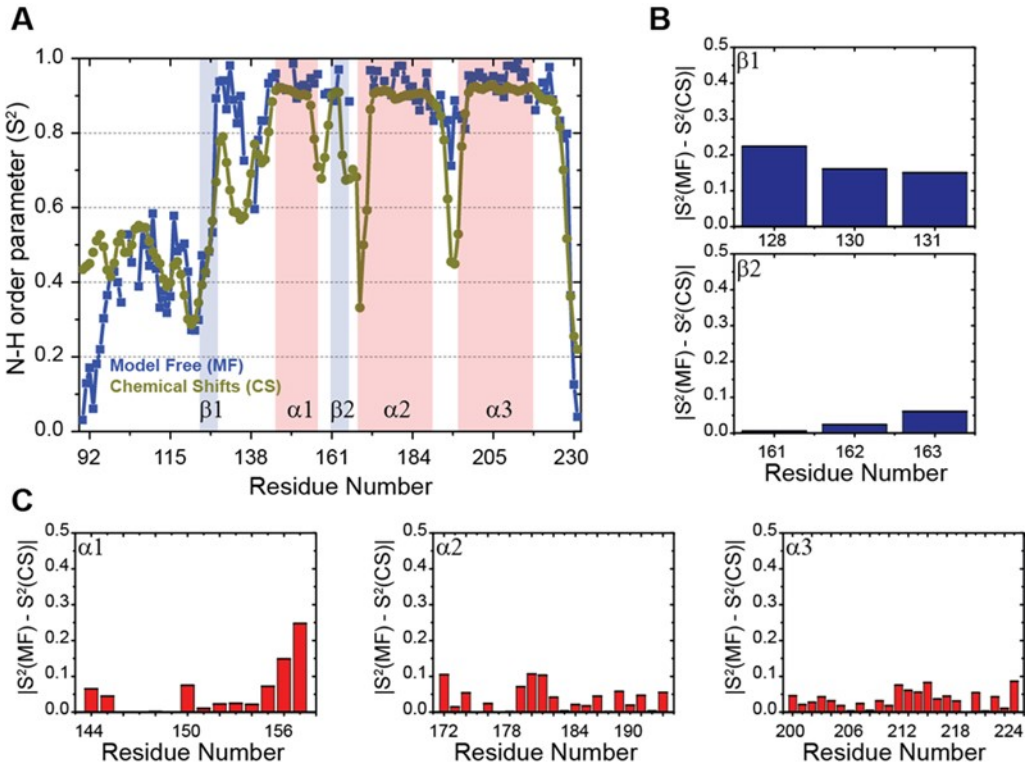

Fig. 8. Model-free order parameter (S^2) analysis. (A) S^2 values estimated from ^{15}N relaxation measurements (S^2_{MF}) and S^2 obtained from backbone chemical shifts (S^2CS) using RCI method as function of the residue number. (B,C) Absolute value of the difference between $S^2(MF)$ and $S^2(CS)$ for each of the secondary structure elements contained in the globular domain. S^2_{MF} values were estimated using for the flexible region (90-126), a local rotational diffusion model; whereas for the folded region of the C-terminal domain (127-231) a global axially symmetric rotational diffusion model (τc= 11.56 ± 0.11 ns; $D^{\parallel}/D^{\perp}$= 1.38 ± 0.11) was optimized using two-field relaxation data sets (600 and 700 MHz) and the NMR structure of human prion protein (PDB ID: 2LSB).

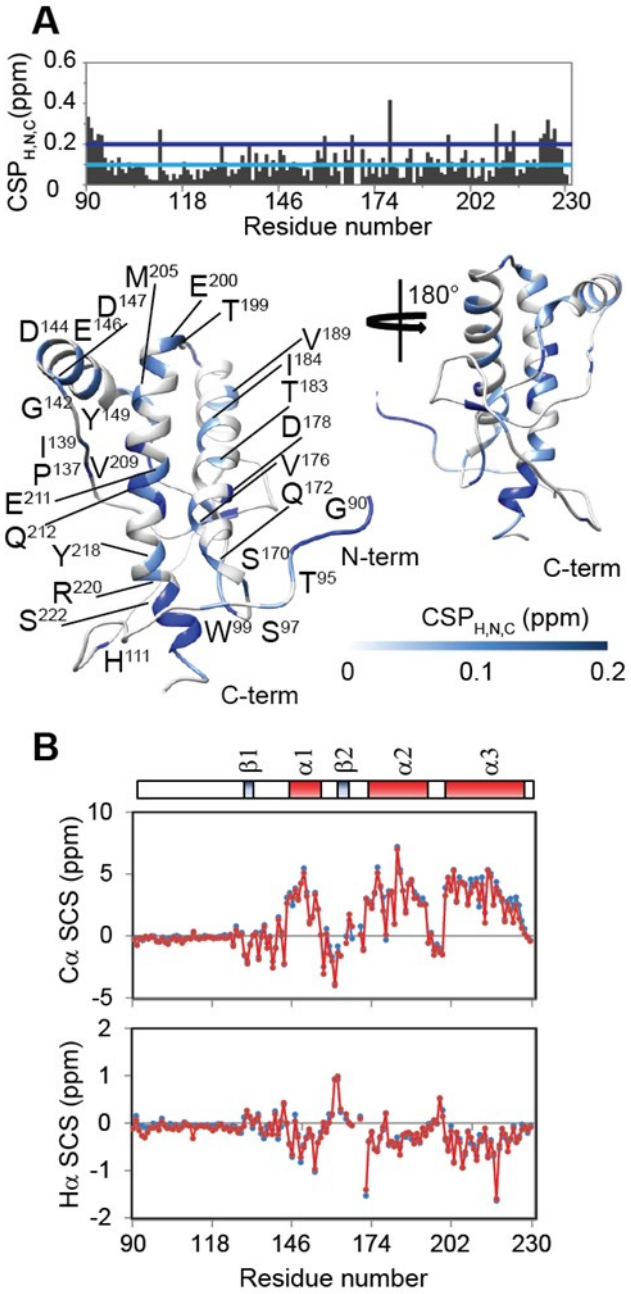

Fig. 9. NMR investigation of the inter-domain coupling. (A) Chemical shift changes (ppm) observed for the C-terminal domain upon deletion of the N-terminal domain. The CSP values ($\Delta_{H,N,C}$) are plotted versus the primary sequence and are mapped onto HuPrP(90-231) NMR structure. Residues with weighted average ^{1}H, ^{15}N and ^{13}C chemical shift perturbation higher than the CSP_{avg} and CSP_{avg} + SD are shown in light blue and blue, respectively. (B) Hα (upper) and Cα (lower) secondary chemical shifts (Gly^{90}-Ser^{231}) for truncated (blue) and full-length (red) HuPrP.

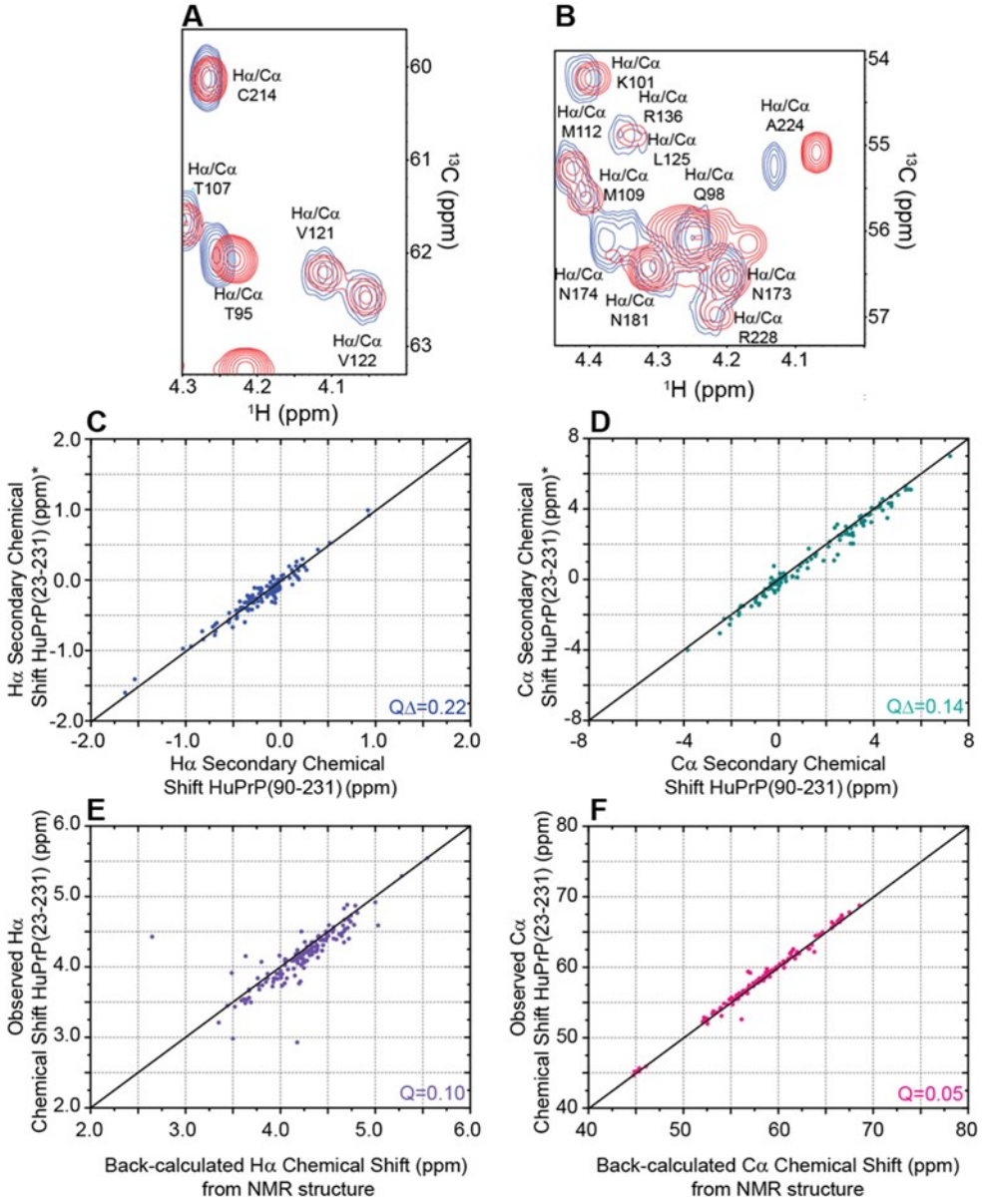

Fig. 10. NMR structural details of the inter-domain coupling. (A, B) Overlay of ^{1}H-^{13}C HSQC spectra of HuPrP(23-231) (red) and HuPrP(90-231) (blue) acquired on 600 MHz spectrometer at 25°C pH 5.5. (C, D) Correlation plots of Hα (yellow) and Cα (green) secondary chemical shifts obtained for the HuPrP(90-231) with respect those measured for the residues of HuPrP(23-231) . Only the data related to the region Gly^{90}- Ser^{231} of the full-length prion protein were included in the analysis. (E, F) Plot of measured Hα and Cα chemical shifts for the full-length prion protein versus those back-calculated from the representative conformer of the C-terminal-domain NMR structure (PDB ID 2LSB).

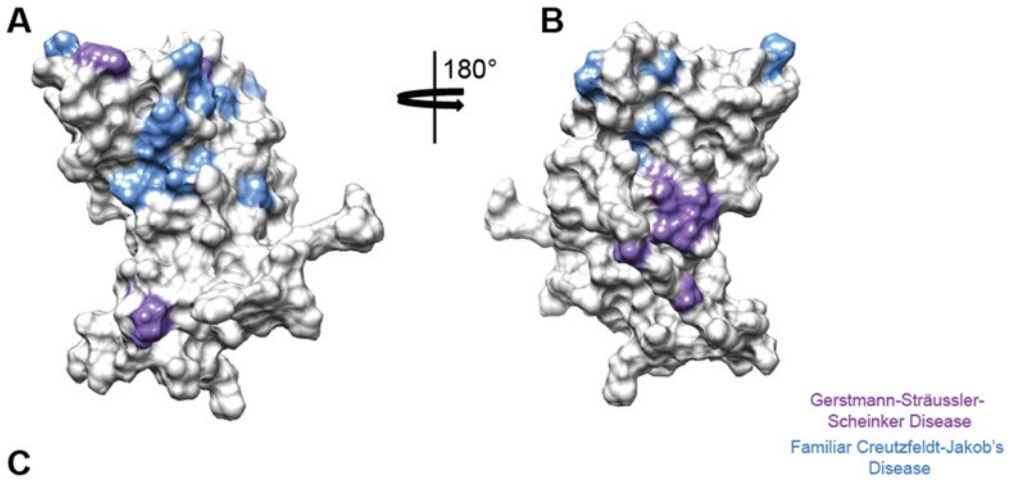

C

Disease	Familial pathogenic mutations
Familial Creutzfeldt-Jakob's	R148N
	D178N(M129V)
	V180I
	T183A
	H187R
	T188K,T188R,T188A
	T193I
	E196K
	E200K
	V203I
	R208H
	V210I
	E211Q
	Q212P
	Q217R
	M232R,M232T
	P238S
Gerstmann-Sträussler-Sckeinker	P102L
	P105L, P105T, P105S
	G114V
	A117V
	G131V
	S132I
	A133V
	Y145stop
Fatal Familial Insomnia	D178N(M129V)

Fig. 11. Human Prion Familiar pathogenic mutations. (A, B) Mapping of HuPrP familial pathogenic mutations onto the C-terminal domain surface in two orientations (see insert) rotated by 180° around the z-axis. The pathogenic mutations related to Familiar Creutzfeldt-Jakob's and Gerstmann-Sträussler-Scheinker disease are painted in light blue and light purple, respectively. (C) The table contains all familiar pathogenic mutations including those related to the Fatal Familial Insomnia (light grey).

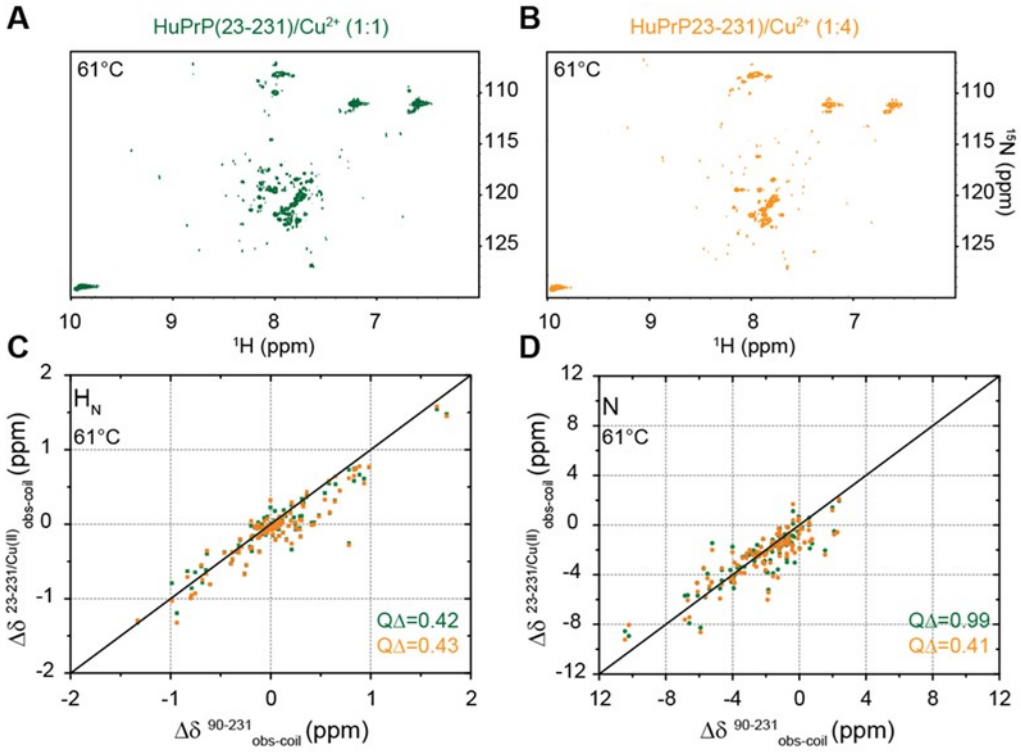

Fig. 12. NMR thermal unfolding of the HuPrP(23-231) upon addition of copper. (A, B) ^{1}H-^{15}N HSQC used to monitor the thermal unfolding of HuPrP(23-231) in the presence of 1 (A) and 4 (B) equivalent(s) of copper at 61°C. (C,D) Correlation plots of HN and N secondary chemical shifts obtained for β-PrPI with respect those observed at 61°C for HuPrP(23-231)/Cu^{2+}(1:1) (dark green) and (1:4) (orange).

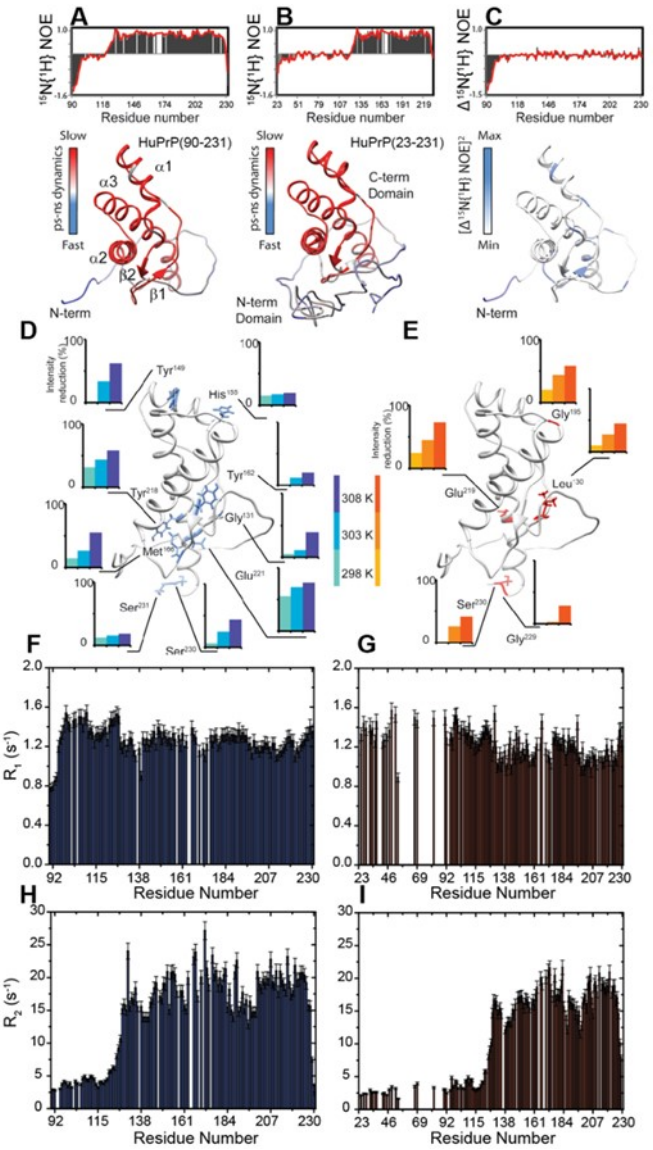

Fig. 13. Comparison of backbone motions of HuPrP(90-231) and HuPrP(23-231) probed by NMR at 600 MHz. (A, B, C) Picosecond-nanosecond mobility of backbone amide bond vector measured via ^{15}N[1H]NOE. Residue-specific ^{15}N[^{1}H]NOE values as proxies of ps-ns mobility for HuPrP(90-231) (A) and HuPrP(23-231) (B). The differences in NOEs between HuPrP(90-231) and the full-length protein are also reported (C). The NOEs are mapped onto the representative NMR structure of the globular domain (90-231) (PDB ID CODE: 2LSB). (D, E) ^{1}H-^{15}N NMR signals broadening analysis. Residues of HuPrP(90-231) (D) and HuPrP(23-231) (E) showing a detectable signal broadening at increasing of temperature in the ^{1}H,^{15}N HSQC spectra are mapped onto the NMR structure of the C-terminal domain (PDB ID: 2LSB). The ^{1}H,^{15}N signal intensities at 25°C (cyan), 30°C (light blue) and 35 °C (violet), relative to the intensity at 15°C, are shown as inserts. (F-I) NMR Relaxation rates of HuPrP(23-231) and HuPrP(90-231). (F, G) ^{15}N R_1 for HuPrP(90-231) (blue) and HuPrP(23-231) (red). (H, I) ^{15}N R_2 for HuPrP(90-231) (blue) and HuPrP(23-231) (red). The relaxation experiments were performed on 600 MHz at 25°C, pH 5.5.

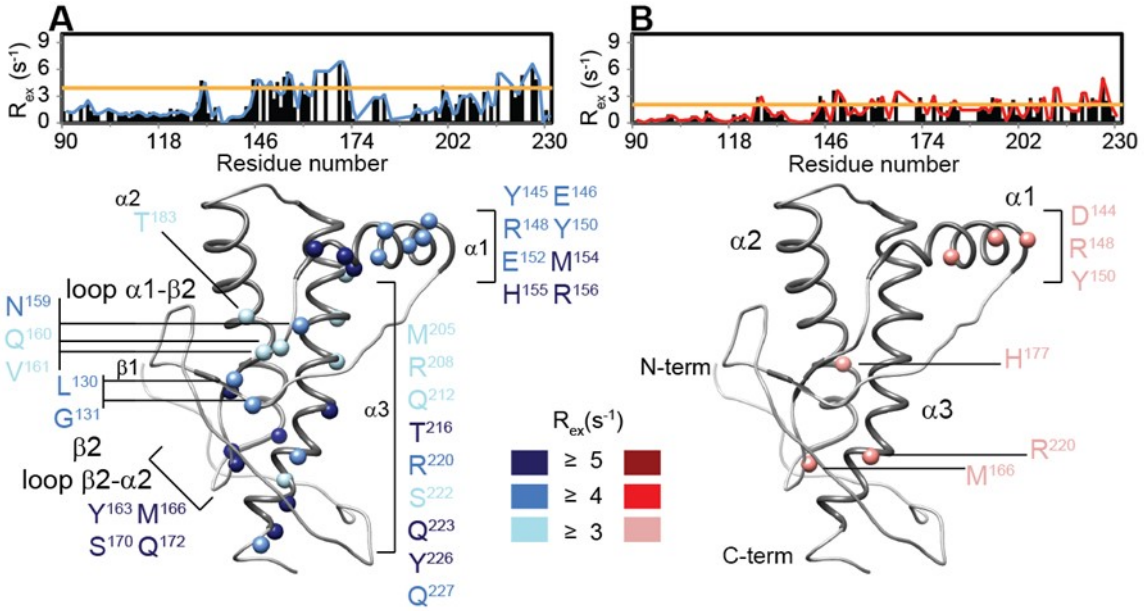

Fig. 14. Millisecond-to-microsecond dynamics of prion protein. (A, B) (upper) Rex values as function of residue number for HuPrP(23-231) and HuPrP(90-231). (lower) Mapping of residues showing significant Rex rates onto the C-terminal domain structure. (A) Residues of HuPrP(90-231) with Rex ≥ 5 s^{-1} (2SD above the mean value (Rex_{avg})) (blue), ≥ 4 s^{-1} (SD above Rex_{avg}) (light blue), ≥ 3 s^{-1} (Rex_{avg}) (cyan); (B) Residues of HuPrP(23-231) with Rex values ≥ 3 s^{-1} (light red).

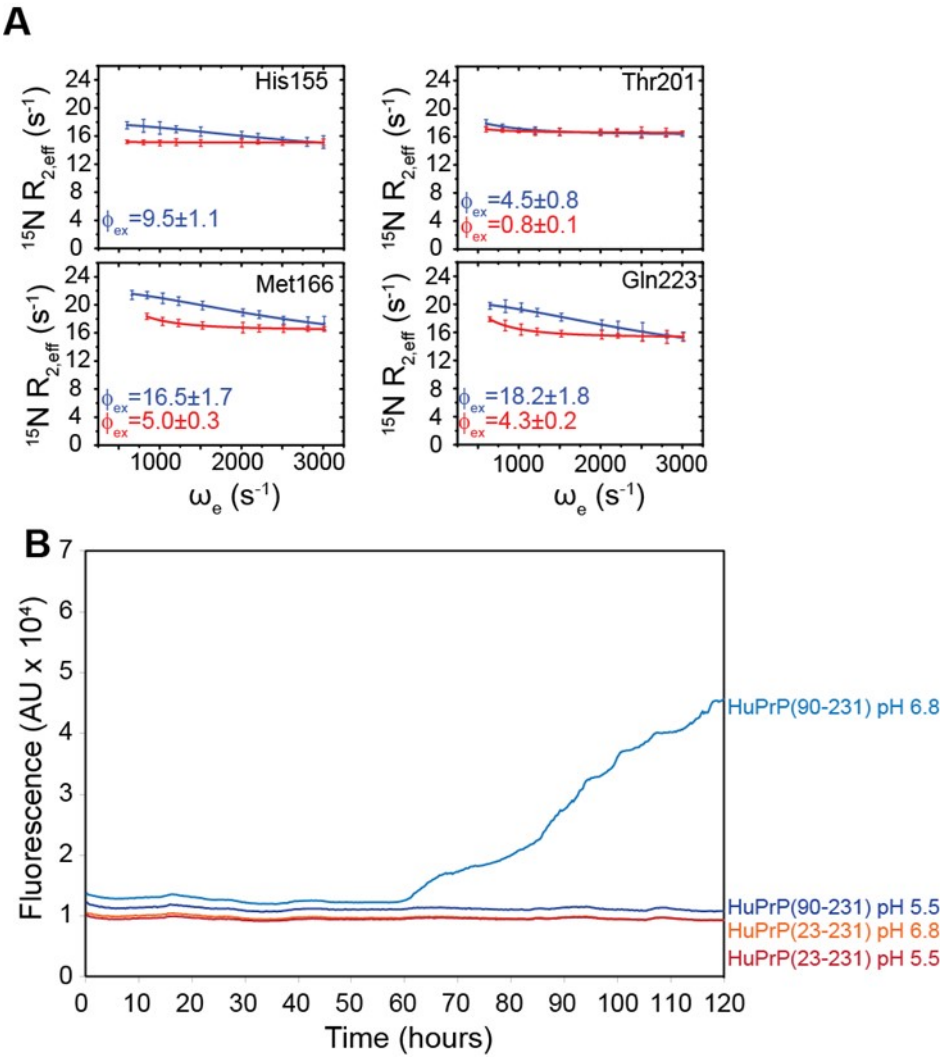

Fig. 15. NMR Relaxation dispersion and ThT Fluorescence experiments. (A) Best fit curves to a two-site exchange model assuming a common motion for His^{155}, Met^{166}, Thr^{201} and Gln^{223} of HuPrP(90-231) (blue) (kex= 2197 ± 138 s^{-1}) and HuPrP(23-231) (red) (kex = 313 ± 23 s^{-1}). (B) HuPrP(90-231) and HuPrP(23-231) were induced to aggregate by alternating cycles of incubation and shaking, at 25°C. Average ThT fluorescence intensity was plotted against time.

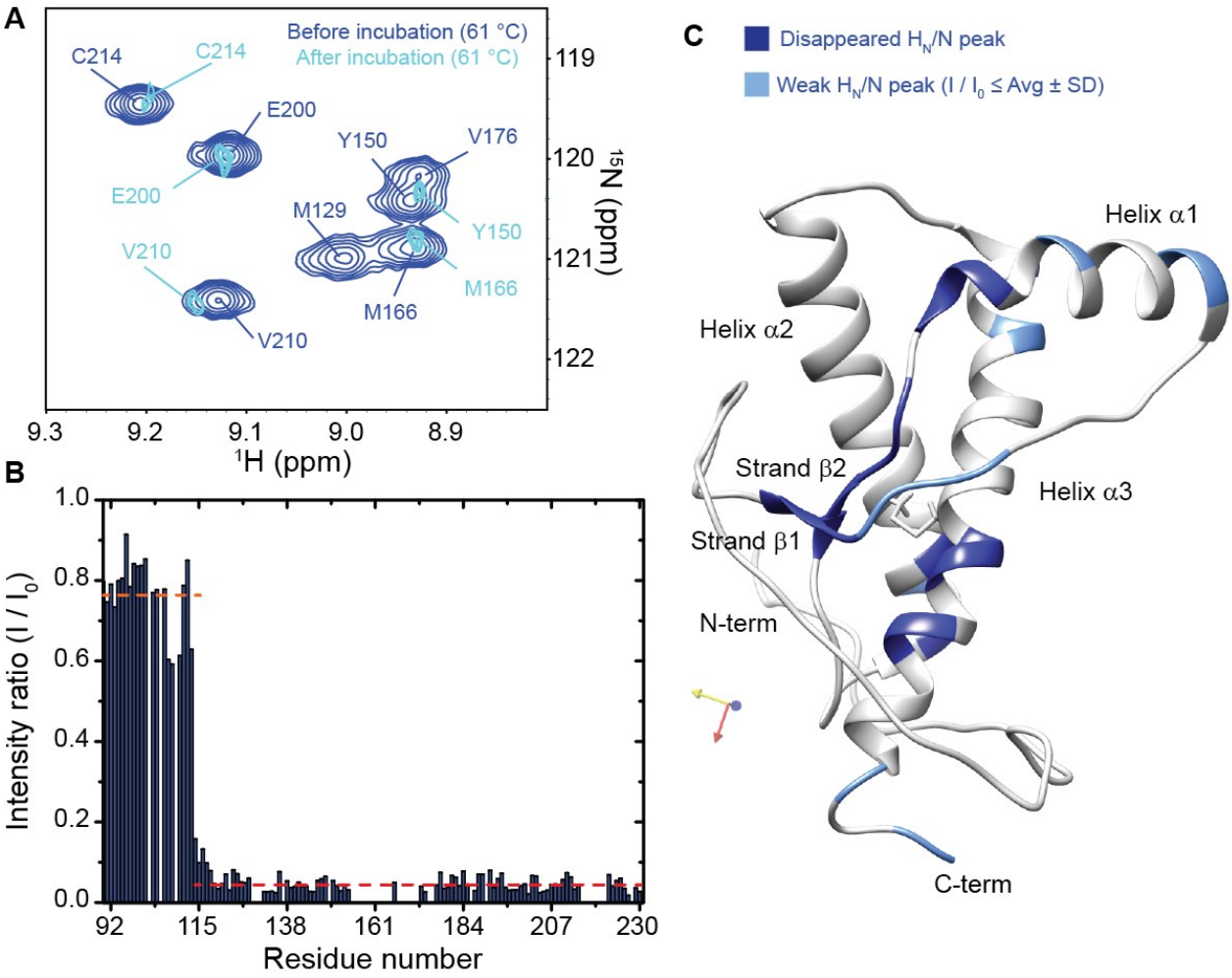

Fig. 16. NMR signal perturbation mapping of β-PrPI oligomerisation interface. (A) Overlay of ^{1}H-^{15}N HSQC spectra of HuPrP(90-231) acquired at 25 °C before (blue) and after (cyan) incubation at 61 °C (15 hours). (B) Ratio between signal intensity after 15 h incubation at 61 °C (I) and intensity of the HuPrP(90-231) monomer plotted against residue number. The mean I/I_0 ratio for the region 90-113 is reported with orange dashed line; whereas the average I/I_0 value for the region 114-231 is depicted as red dashed line. (C) Mapping of oligomerisation interface. Residues with I/I_0 ratios lower than average ± SD (standard deviation) are colored in light blue; whereas the residues for which the HN/N peaks disappeared are depicted as blue.

Protein	N-U	N-I-U	*p*-value (*F-test*)
HuPrP(90-231)pH 5.5*(10μM)	-----	Tm_1= 52 ± 1 Tm_2= 74 ± 2	<0.001
HuPrP(90-231)pH 5.5*(20μM)	-----	Tm_1= 55 ± 2 Tm_2= 72 ± 2	0.00857
HuPrP(90-231)pH 5.5*(30μM)	-----	Tm_1= 52 ± 2 Tm_2= 75 ± 2	<0.001
HuPrP(90-231)pH 5.5*(80μM)	-----	Tm_1= 55 ± 1 Tm_2= 72 ± 1	<0.001
HuPrP(90-231)pH 6.8#(10μM)	-----	Tm_1= 56 ± 3 Tm_2= 70 ± 1	<0.001
HuPrP(90-231)pH 6.8#(20μM)	-----	Tm_1= 55 ± 2 Tm_2= 69 ± 1	0.00685
HuPrP(90-231)pH 6.8#(30μM)	-----	Tm_1= 59 ± 3 Tm_2= 68 ± 2	<0.001
HuPrP(23-231)pH 5.5* (10μM)	Tm= 69 ± 2	-----	<0.001
HuPrP(23-231)pH 5.5* (20μM)	Tm= 69 ± 2	-----	<0.001
HuPrP(23-231)pH 5.5* (30μM)	Tm= 69 ± 3	-----	<0.001
HuPrP(23-231)pH 5.5* (80μM)	Tm= 69 ± 3	-----	<0.001
HuPrP(23-231)pH 6.8# (10μM)	Tm= 59 ± 1	-----	<0.001
HuPrP(23-231)pH 6.8# (20μM)	Tm= 59 ± 1	-----	<0.001
HuPrP(23-231)pH 6.8# (30μM)	Tm= 59 ± 1	-----	<0.001
HuPrP(23-231)pH 5.5‡ (10μM)	Tm= 69 ± 2	-----	<0.001
HuPrP(23-231)/Cu^{2+} (1:1) pH 5.5‡	-----	Tm_1= 51 ± 4 Tm_2= 73 ± 4	<0.001
HuPrP(23-231)/Cu^{2+} (1:4) pH 5.5‡	-----	Tm_1= 58 ± 2 Tm_2= 75 ± 1	<0.001

Table 1. Thermal stability of prion samples at different pHs and protein concentrations estimated by CD data. Melting temperatures (Tm) (°C) of HuPrP(90-231) and HuPrP(23-231) unfolding processes determined from equilibrium CD experiments at different pH values and at increasing protein concentration. Measurements were performed using acetate*, phosphate# and MES‡ buffer with the same ionic strength. The *p-value* of the statistical *F-test* applied to identify the best model, between the two- and three-state, for the description of the folding mechanism is also reported.

Protein	A.I. Initial	$\theta_{222}/\theta_{219}$ Initial	A.I. After heating	$\theta_{222}/\theta_{219}$ After heating	Reversibility (%)
HuPrP(90-231)pH 5.5* (10μM)	<10	0.9 (1.0)*	<10	0.9	97
HuPrP(90-231)pH 5.5* (20μM)	<10	0.9	<10	0.9	77
HuPrP(90-231)pH 5.5* (30μM)	<10	0.9	<10	0.9	69
HuPrP(90-231)pH 6.8$^{\#}$(10μM)	<10	0.9	<10	0.9	76
HuPrP(90-231)pH 6.8$^{\#}$(20μM)	<10	0.9	<10	0.9	60
HuPrP(90-231)pH 6.8$^{\#}$(30μM)	<10	0.9	<10	0.9	48
HuPrP(23-231)pH 5.5* (10μM)	<10	0.9	<10	0.9	100
HuPrP(23-231)pH 5.5* (20μM)	<10	0.9	<10	0.9	87
HuPrP(23-231)pH 5.5* (30μM)	<10	0.9	<10	0.9	76
HuPrP(23-231)pH 6.8$^{\#}$ (10μM)	<10	0.9	<10	0.9	83
HuPrP(23-231)pH 6.8$^{\#}$ (20μM)	<10	0.9	<10	0.9	50
HuPrP(23-231)pH 6.8$^{\#}$ (30μM)	<10	0.9	<10	0.9	40
HuPrP(23-231)pH 5.5‡ (10μM)	<10	0.9	<10	0.9	94
HuPrP(23-231)/Cu^{2+} (1:1) pH 5.5‡	<10	0.9	<10	0.9	95
HuPrP(23-231)/Cu^{2+} (1:4) pH 5.5‡	<10	0.9	<10	0.9	80

Table 2. Reversibility, Aggregation Index and $\theta_{222}/\theta_{219}$ values obtained for all investigated prion samples. The (*) indicates the θ222/θ219 obtained from the ellipticity values predicted from the NMR structure. A.I. values below 10 usually represents solutions with insignificant amount of aggregate. Measurements were performed using acetate*, phosphate# and MES‡ buffer with the same ionic strength.

Residue	Region	Protein	$k_{ex}(s^{-1})$	$R_2^0(s^{-1})$	$\Phi_{ex}(x10^3\ (s^{-1})^2)$
Gly^{131}	β-strand (β1)	HuPrP(90-231)	2429 ± 277	17.7 ± 0.5	13.7 ± 2.6
		HuPrP(90-231)E219K	399 ± 21	14.7 ± 0.1	6.1 ± 0.2
		HuPrP(23-231)	339 ± 44	15.6 ± 0.5	1.3 ± 0.1
Tyr^{150}	α-helix (α1)	HuPrP(90-231)	2762 ± 296	11.4 ± 0.7	18.7 ± 3.7
		HuPrP(90-231)E219K	353 ± 70	12.3 ± 0.1	5.3 ± 0.6
		HuPrP(23-231)	317 ± 63	13.9 ± 0.1	4.6 ± 0.5
Glu^{152}		HuPrP(90-231)	2181± 307	13.6 ± 0.8	16.8 ± 3.7
		HuPrP(90-231)E219K	-----	-----	-----
		HuPrP(23-231)	-----	-----	-----
His^{155}	loop(α1- β2)	HuPrP(90-231)	2597 ± 214	13.0 ± 0.4	12.5 ± 1.8
		HuPrP(90-231)E219K	422 ± 45	13.9 ± 0.1	4.2 ± 0.2
		HuPrP(23-231)	-----	-----	-----
Gln^{160}	β-strand (β2)	HuPrP(90-231)	2997 ± 365	11.5 ± 0.8	19.0 ± 4.5
		HuPrP(90-231)E219K	-----	-----	-----
		HuPrP(23-231)	-----	-----	-----
Met^{166}	loop(β2-α2)	HuPrP(90-231)	2567 ± 250	13.8 ± 0.7	21.2 ± 3.6
		HuPrP(90-231)E219K	273 ± 77	14.7 ± 0.1	9.5 ± 2.1
		HuPrP(23-231)	302 ± 144	16.4 ± 0.1	5.2 ± 1.9
Asn^{181}	α-helix (α2)	HuPrP(90-231)	1198 ± 93	15.6 ± 0.1	2.3 ± 0.2
		HuPrP(90-231)E219K	334 ± 39	13.9 ± 0.1	3.0 ± 0.2
		HuPrP(23-231)	287 ± 42	15.9 ± 0.1	1.6 ± 0.2
Glu^{200}	turn(α2-α3)	HuPrP(90-231)	483 ± 21	16.8 ± 0.1	4.7 ± 0.1
		HuPrP(90-231)E219K	332 ± 32	13.2 ± 0.1	5.6 ± 0.3
		HuPrP(23-231)	268 ± 43	14.1 ± 0.1	3.4 ± 0.3
Thr^{201}	α-helix (α3)	HuPrP(90-231)	506 ± 80	16.3 ± 0.1	1.9 ± 0.1
		HuPrP(90-231)E219K	400 ± 31	14.7 ± 0.1	2.7 ± 0.1
		HuPrP(23-231)	420 ± 64	16.6 ± 0.1	0.7 ± 0.1
Gln^{223}	C-terminal	HuPrP(90-231)	2571 ± 282	11.4 ± 0.9	23.4 ± 4.5
		HuPrP(90-231)E219K	401 ± 29	13.8 ± 0.1	3.5 ± 0.2
		HuPrP(23-231)	325 ± 59	15.3 ± 0.1	4.2 ± 0.5

Table 3. Relaxation Dispersion data analysis. Individual fit parameters obtained from $R_2^{eff}(\omega e)$ relaxation dispersion data for HuPrP(90-231), HuPrP(90-231)E219K and HuPrP(23-231).

Residue	Region	Protein	$R_2^0(s^{-1})$	$\Phi_{ex}(x10^3\ (s^{-1})^2)$	χ^2global/ χ^2ind
Gly^{131}	β-strand (β1)	HuPrP(90-231)	18.1 ± 0.3	11.7 ± 1.3	1.1
		HuPrP(90-231)E219K	14.7 ± 0.1	6.3 ± 0.2	1.2
		HuPrP(23-231)	15.6 ± 0.1	1.3 ± 0.1	0.9
Tyr^{150}	α-helix (α1)	HuPrP(90-231)	12.6 ± 0.3	12.8 ± 1.4	2.9
		HuPrP(90-231)E219K	12.3 ± 0.1	5.1 ± 0.1	1.0
		HuPrP(23-231)	13.9 ± 0.1	4.7 ± 0.2	1.0
Glu^{152}		HuPrP(90-231)	13.6 ± 0.4	17.0 ± 1.8	1.0
		HuPrP(90-231)E219K	-----	-----	-----
		HuPrP(23-231)	-----	-----	-----
His^{155}	loop(α1-β2)	HuPrP(90-231)	13.6 ± 0.3	9.5 ± 1.1	2.0
		HuPrP(90-231)E219K	13.9 ± 0.1	4.3 ± 0.1	1.0
		HuPrP(23-231)	-----	-----	
Gln^{160}	β-strand (β2)	HuPrP(90-231)	13.0 ± 0.3	11.0 ± 1.2	2.8
		HuPrP(90-231)E219K	-----	-----	-----
		HuPrP(23-231)	-----	-----	-----
Met^{166}	loop(β2-α2)	HuPrP(90-231)	14.8 ± 0.4	16.5 ± 1.7	1.4
		HuPrP(90-231)E219K	14.7 ± 0.1	7.5 ± 0.2	1.8
		HuPrP(23-231)	16.4 ± 0.1	5.0 ± 0.3	1.9
Asn^{181}	α-helix (α2)	HuPrP(90-231)	15.1 ± 0.2	4.6 ± 0.8	2.2
		HuPrP(90-231)E219K	13.9 ± 0.1	2.9 ± 0.1	1.6
		HuPrP(23-231)	15.9 ± 0.1	1.5 ± 0.1	1.2
Glu^{200}	turn(α2-α3)	HuPrP(90-231)	15.1 ± 0.3	10.3 ± 1.2	334.7
		HuPrP(90-231)E219K	13.1 ± 0.1	5.3 ± 0.1	1.3
		HuPrP(23-231)	14.1 ± 0.1	3.0 ± 0.2	1.3
Thr^{201}	α-helix (α3)	HuPrP(90-231)	15.5 ± 0.2	4.5 ± 0.8	2.8
		HuPrP(90-231)E219K	14.7 ± 0.1	2.8 ± 0.1	1.0
		HuPrP(23-231)	16.6 ± 0.1	0.8 ± 0.1	2.0
Gln^{223}	C-terminal	HuPrP(90-231)	12.5 ± 0.4	18.2 ± 1.8	1.8
		HuPrP(90-231)E219K	13.7 ± 0.1	3.7 ± 0.1	1.3
		HuPrP(23-231)	15.3 ± 0.1	4.3 ± 0.2	1.0

Table 4. Global fit parameters obtained from $R_2^{eff}(\omega e)$ relaxation dispersion measurements HuPrP(90-231) and HuPrP(23-231). The parameters were estimated by fitting the ^{15}N $R_1\rho$ relaxation dispersion data to a two-site exchange model assuming a common motion for HuPrP(90-231) (kex = 2197 ± 138 s^{-1}), HuPrP(90-231)E219K (kex = 373 ± 15 s^{-1})and HuPrP(23-231) (kex = 313 ± 23 s^{-1}).

Cluster A

Residue	Region	Protein	$R_2^0(s^{-1})$	$\Phi_{ex}(x10^3\ (s^{-1})^2)$	χ^2global/ χ^2ind
Gly^{131}	β-strand (β1)	HuPrP(90-231)	17.5 ± 0.3	14.4 ± 1.2	1.0
Tyr^{150}	α-helix (α1)	HuPrP(90-231)	11.9 ± 0.3	15.7 ± 1.2	1.5
Glu^{152}		HuPrP(90-231)	12.8 ± 0.3	20.9 ± 1.6	1.1
His^{155}	loop(α1- β2)	HuPrP(90-231)	13.2 ± 0.2	11.7 ± 0.9	1.1
Gln^{160}	β-strand (β2)	HuPrP(90-231)	12.5 ± 0.2	13.7 ± 1.1	1.7
Met^{166}	loop(β2-α2)	HuPrP(90-231)	14.0 ± 0.3	20.3 ± 1.5	1.0
Gln^{223}	C-terminal	HuPrP(90-231)	11.6 ± 0.3	22.3 ± 1.6	1.1

Table 5. Global fit parameters for the cluster A obtained from $R_2^{eff}(\omega e)$ relaxation dispersion measurements for HuPrP(90-231). The parameters were estimated by fitting the ^{15}N $R_1\rho$ relaxation dispersion data to a two-site exchange model assuming a common motion for HuPrP(90-231) (kex = 2502 ± 106 s^{-1}).

	$\Sigma\chi^2$	AICc	BIC
All	27	78	121
Cluster A	5.4	44	69

Table 6. Statistical analysis of relaxation dispersion fits for HuPrP(90-231). Lowest AICc and BIC indicate that statistically the cluster A is the best model.